Biological and Medical Applications of Materials and Interfaces

Sensitive plasmonic detection of miR-10b in biological samples by using enzyme-assisted target recycling and developed LSPR probe

Ji Sun Ki, Hyo young Lee, Hye yeong Son, Yong-Min Huh, and Seungjoo Haam

ACS Appl. Mater. Interfaces, **Just Accepted Manuscript** • DOI: 10.1021/acsami.9b03005 • Publication Date (Web): 08 May 2019

Sensitive plasmonic detection of miR-10b in biological samples by using enzyme-assisted target recycling and developed LSPR probe

Jisun Ki[1], Hyo young Lee[1], Hye yeong Son[2], Yong-Min Huh[2,*], Seungjoo Haam[1,*]

[1]Department of Chemical and Biomolecular Engineering, Yonsei University, Yonsei-ro 50, Seoul 120-749, South Korea
[2]Department of Radiology, College of Medicine, Yonsei University, Seoul 120-752, South Korea
Fax: +82-(2)-312-6401 E-mail address: ymhuh@yuhs.ac.kr, haam@yonsi.ac.kr

KEYWORDS:, miRNA sensing, miR-10b, LSPR, gold nanoparticle, DSN, hybridization chain reaction

ABSTRACT

A portable and non-labeled plasmonic biosensor was advanced to enable the sensitive and selective detection of microRNA(miRNA) in biological sample. miRNAs can act on several key cellular processes including cell differentiation, cell cycle progression and function as oncogenes. Detection of circulating miRNAs, especially in blood or urine samples, allows noninvasive and simple diagnosis of disease. Herein, we report a localized surface plasmon resonance sensor (LSPR) based on enzyme assisted target recycling system and developed LSPR probe for the detection of gastric cancer relevant miRNAs, miR-10b. Sensitivity of the sensor was improved by increasing the concentration of the signal amplifying agent using the duplex specific nuclease (DSN) and by strongly binding the developed LSPR probe, tannic acid capping gold nanoparticles, to the DNA. Under optimal conditions, miR-10b detection could be realized in the range of 5 pM-10 nM with a detection limit of 2.45 pM. This integrated detection system represents an approach to sensitive detection of miRNAs and offer great applications in personalized medicine and monitoring of cancer.

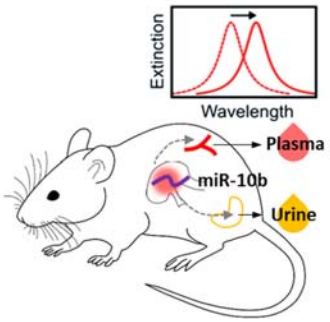

INTRODUCTION

MicroRNAs (miRNAs) are a class of endogenous non-coding small RNAs that regulate gene expression and have attention over the past decades from the fundamental biological processes and biomedical research fields.[1-2] Recent studies have demonstrated that involvement of miRNAs in diverse aspects of diseases including diabetes as well as brain function and cancer.[3-4] Moreover, miRNAs are potential non-invasive biomarkers to monitor the body's pathophysiological status because they are released from the distant organs constitute and circulated in body-fluid.[5-8] Therefore, sensitive sensing of miRNAs in biological samples such as blood or urine may provide individualized therapeutic strategies and facilitate precision medicine.[9-11] In order to apply miRNA detection technology in the medical diagnosis field, a reasonable and facile system is required instead of expensive equipment, such as a polymerase chain reaction (PCR) and fluorescence spectroscopy.[12-13]

The localized surface plasmon resonance (LSPR) is one of the optical properties of metal nanoparticles, which occur when the incident photon frequency is resonant with the collective oscillation of the conduction electrons on the metal surfaces.[14-15] Label-free and high sensitive sensing of biomolecules such as bacteria, protein and gene are possible using the LSPR properties and also LSPR have advantages of low-cost and easy-to-use.[16-18] Moreover, duplex specific nuclease (DSN) generating signal-amplifying mechanism may provide the sensitivity of low abundance miRNAs in the biological samples and the selectivity of the target miRNA sequence homology among the family members.[19] DSN can cleave double-stranded DNA or DNA in RNA-DNA heteroduplexes with no significant cleavage of single-stranded DNA or single- or double-stranded RNA.[20] Moreover, DSN exhibits a high selectivity for miRNA family members, even for a single-base mismatch owing to the discrimination ability of the DSN between completely and incompletely matched short duplexes. To further improve the sensitivity, a DNA-mediated self-assembly amplification method can provide highly ordered DNA double helixes via a triggered cascade of DNA polymerization by an initiator or target molecules.[21-22] Therefore, the signaling molecules can be attached to these helixes with a precisely controlled density, which could be beneficial for the final amplification efficiency.

As shown in Scheme 1, the proposed protocol for the monitoring of miRNA-10b involves DSN-assisted target recycling production of numerous intermediate DNA fragments (Scheme 1A). miR-10b was highly correlated with size of tumor, Lauren classification, depth of invasion, metastasis and prognosis in gastric cancer.[23-25] Subsequently, the intermediate DNA induced formation of super-sandwich self-assemblies allowed LSPR peak monitoring of the adsorbed tannic acid capped gold nanoparticles via hydrogen bonding (Scheme 1B). The tannic acid capped gold nanoparticles

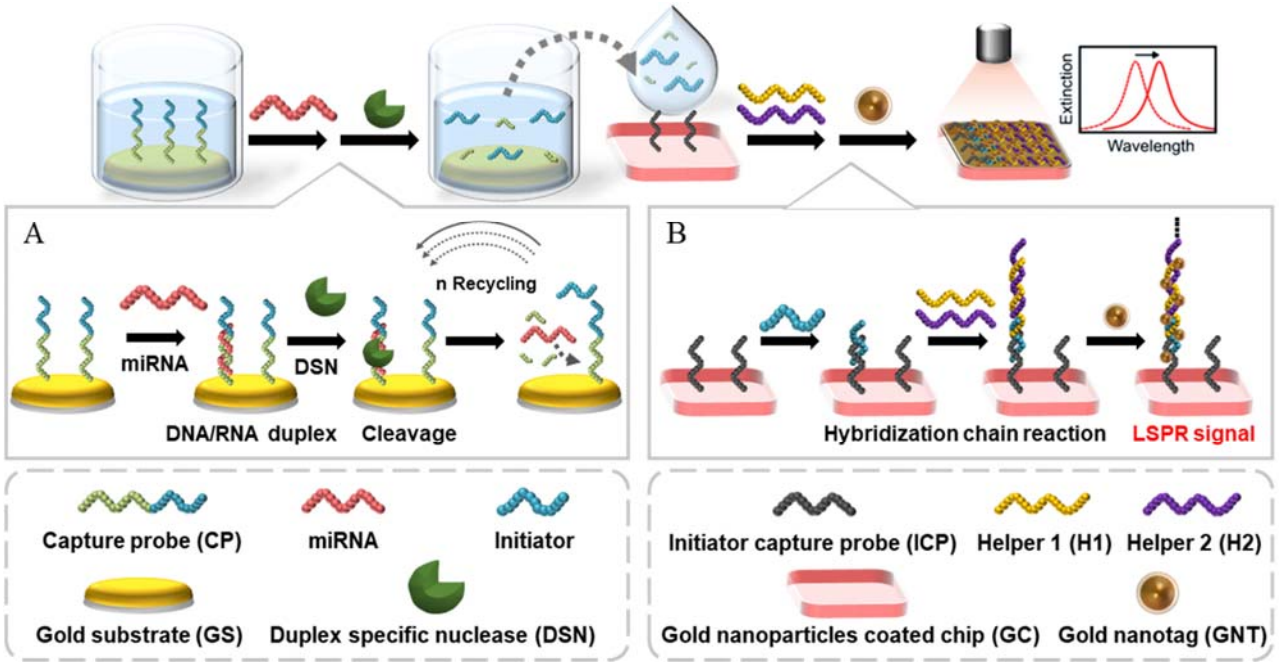

Scheme 1. The principle of the hybrid signal amplification for LSPR-based miRNA sensing. (A) Duplex specific nuclease assisted target miRNA recycling and generation of intermediate single strand DNA, initiator probe. (B) Initiator probe induced formation of the DNA sandwich assemblies.

were developed in conventional LSPR probes and contributed to enhance the sensitivity of the LSPR sensing system. Therefore, the corresponding absorption spectrum of the LSPR chip indicated that with an increase of the miRNA amount, the miRNA could be determined based on the ratiometric readout with an intrinsic self-calibration of the system. This assay is promising for applications in clinical diagnosis.

RESULTS

Characterization of enzyme-assisted target recycling

To demonstrate the developed sensing platform, microRNA-10b (miR-10b) was selected as the model target, which is overexpressed in human gastric cancers. Thus, as shown in Supporting Information Table S1, the capture probe (CP) was consisted of a captured region complementary to miR-10b and an initiator region released from capture probes from cleavage reaction with DSN. The CP was designed with a thiol moiety, and the CP bound to the gold substrate through S-Au bonding (CP/GS). To confirm the CP conjugation on the gold substrate, CP/GS was further characterized by X-ray photoelectron spectroscopy (XPS) (Figure S1). The S2p spectrum exhibited two distinct peaks at 161.8 eV and 163.0 eV with a 2:1 area ratio and splitting of 1.2 eV, which indicated that the thiol groups were bound to the gold chip by forming an S-Au bond, and there were no unbound thiol groups on the sensing surface. The peaks of N1s and P2p are unique signals for single-stranded DNA sequences because the N and P elements contain only phosphate groups and nucleobase, respectively. The splitting peaks of O1s suggested that the O element was present in at least two valence states, which further validated that there was single-stranded DNA on the sensing surface.

In the presence of a miR-10b, the captured region of CP bound miR-10b and the DSN recognized the partial DNA/RNA heteroduplex between the CP and miR-10b and cleaved only the captured region of the CP in the heteroduplex. Therefore, the initiator probe of the CP was derived from the surface of the gold substrate, and the miR-10b participated in the next hybridization with other CP. The capture probe modified fluorophore (cy3) was applied at the 5-terminal (CP-cy3), and DSN-assisted target recycling was confirmed by fluoroscopy. To advance the performance of the designed biosensor, the experimental conditions were optimized. The amount and reaction time of the DSN were the main factors affecting the analytical performance of the sensing system (Figure S2). The fluorescence signals were measured for the addition of 0.01, 0.05, 0.1, 0.2, 0.4 U DSN in the DSN reaction buffer in the presence of miR-10b. Then, the reaction time of the loop amplification in the presence of the DSN and miR-10b was optimized. The optimized amount of DSN enzymes was 0.2 U, and the optimal reaction time was 30 min. Because the enzyme reaction was saturated at 0.2 U, the subsequent experiment was performed at this condition.

To further evaluate the miRNA sensing ability of CP-cy3 conjugated on the gold substrate (CP-cy3/GS), the sensitivity and selectivity were analyzed under the optimal conditions. First, to estimate the target sensitivity of CP-cy3/GS, the limit of detection (LOD) was determined by 0.1-fold serial dilutions of the target miR-10b concentration from 10 pM to 10 nM (Figure 1a). There is no fluorescence signal in absence of the target miR-10b owing to the quenching effect on the gold substrate surfaces, and the LOD of CP-cy3/GS was 100 pM. Second, a significant challenge to developing an effective miRNA assay is the discrimination target among

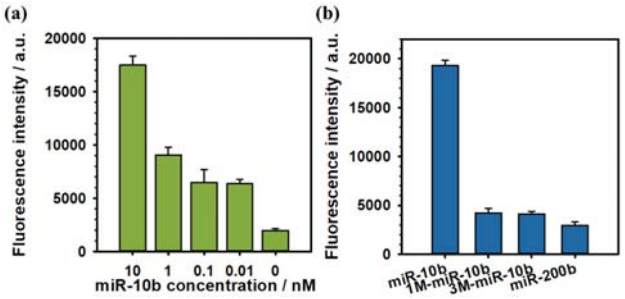

Figure 1. (a) Fluorescence graph of capture probe over a target miR-10b concentration profile (10 pM, 100 pM, 1 nM, 10 nM). (b)Variation of the fluorescence intensity of capture probe in the presence of miR-10b, miR-10b with 1-base mismatches (1M-miR-10b), miR-10b with 3-base mismatches (3M-miR-10b) and miR-200b as non-complementary target.

the highly homologous series of miRNAs. Identifying these miRNAs is important when investigating their expression and understanding their biological functions. DSN is effective at distinguishing between perfectly matched and mismatched duplexes. The selectivity of CP/GS was determined using the following four miRNA sequences: miR-10b, miR-10b with 3-base mismatches (3M-miR-10b), miR-10b with 1-base mismatches (1M-miR-10b) and miR-200b that was non-complementary. As shown in Figure 1b, when the same concentration of various miR-10bs was used, a significant difference in the fluorescence intensity of the miR-10b and other miRNAs was observed. This result clearly suggested that the proposed method was selective and could discriminate between the miRNA family members.

Preparation of the gold nanoparticle coated chip.

The LSPR sensing chip is a combination of a gold nanoparticle coated chip (GC) and initiator capture probes (ICP) that capture the initiator derived from the capture probe. In order to fabricate an LSPR sensing chip producing a precise LSPR signal, a uniform synthesis of the gold nanoparticles (GNPs) is required. The GNPs were synthesized with a controlled size that was useful for sensitive detection, according to a reported method.[26] The pre-synthesized seeds of the GNPs were approximately spherical in shape with an average diameter of 16.6 ± 1.3 nm according to the transmission electron microscope (TEM) images (Figure S3). Furthermore, a growth step was performed for larger sized GNPs because LSPR signal is dependent on the size of the plasmonic nanostructures.[27] Figure 2a shows the TEM images of the GNPs with a 24.8 ± 2.1-nm size obtained after the growth steps. To further improve the shape and uniformity of the particles, ethylenediaminetetraacetic acid (EDTA) was added in the growth steps. The GNPs with a more spherical shape and less size distribution were obtained in the EDTA that those of the GNPs without the addition of EDTA. (Figure S4). To fabricate the GC, (3-aminopropyl)triethoxysilane (APTES) was used as a linker of the amine group to conjugate the GNPs on the glass substrate via an electrostatic interaction. And then, the GC was fabricated by the self-assembly of the GNPs attached to the glass substrate. This result showed the density of gold nanoparticles on GCs increases as the APTES concentration increasing. GCs using various APTES concentrations of 1,5, and 10 % were prepared. The GCs with 5 and 10% concentration showed higher concentrated gold nanoparticles on GCs than with 1% concentration.

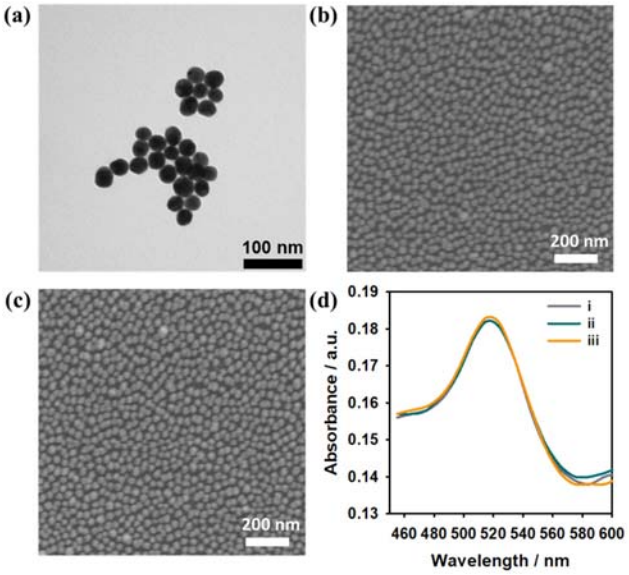

Figure 2. (a) TEM image of the gold nanoparticles (scale bar; 100 nm) and the SEM images of (b) the gold nanoparticle coated chip and (c) gold nanoparticle coated chip with a polydopamine layer (scale bar; 200 nm). (d) UV spectra of the (i) gold nanoparticles in the solution, (ii) gold nanoparticle coated chip, (iii) gold nanoparticle coated chip with a polydopamine layer.

In addition, the optical property of the GC was measured using UV-Vis spectroscopy. The surface plasmon absorption spectrum of the GC with a 1 and 5% concentration of APTES showed a maximum adsorption peak at 520 nm. However, a shift in the adsorption peak was observed in the GC with 10% APTES owing to the aggregation of the nanoparticles on the glass substrate. This was set as a condition because the 5% material had a high density and stability.

Moreover, we applied polydopamine coating to increase stability in various solutions. As a result of experiments under various concentration conditions, the absorbance spectrum according to the concentration showed that the concentration and shift of the LSPR peak were directly proportional (Figure S5). The substrate was unstably synthesized by the self-assembly of dopamine and the coagulation reaction with the GNPs under the high dopamine concentration. Due to this phenomenon, the fluctuation of the peak was severe after repetitive washing. However, without the polydopamine coating, the substrate is unstable under buffer conditions and in the washing process. And Therefore, the optimal synthesis condition of the substrate for generating a uniform LSPR signal was 3.3 mM while maintaining the stability of the GC (Figure S5). As shown in Figure 2c, there was no aggregation and detachment of the GNPs on the GC with polydopamine layer.[28] The UV spectra confirmed that the polydopamine coated GC did not significantly change the optical

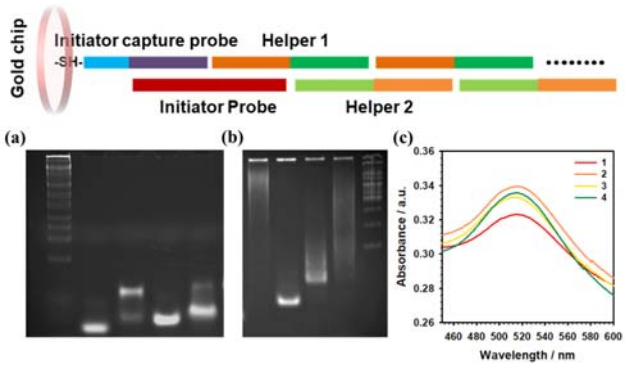

Figure 3. (a) 15% Polyacrylamide gel electrophoresis of reaction products. From left to right: lane 1; DNA ladder, lane 2; Initiator capture probe (ICP), lane 3; Initiator probe (IP), lane 4; Helper 1 (H1), lane 5; Helper 2 (H2) (b) Polyacrylamide gel electrophoresis of reaction products. From left to right: lane 1; Duplex between H1 and H2 (H1/H2), lane 2; Duplex between ICP and IP (ICP/IP), lane 3; DNA polymers composed ICP/IP and H1/H2 (ratio 1:1), lane 4; DNA polymers composed ICP/IP and H1/H2 (ratio 1:5), lane 5; DNA ladder (c) LSPR spectra at each reaction steps. (i) gold nanoparticles coated chip (GC); (ii) Initiator capture probe conjugated GC (GC/ICP), (iii) Initiator probe conjugated GC+ICP (GC/ICP/IP), (iv) DNA self-assembly with H1 and H2 on GC+ICP+IP (GC/ICP/IP/H1/H2).

property compared to the GNP solution and gold-nanoparticle coated LSPR chip (Figure 2d).

Fabrication of the DNA functionalized gold coated chip

When the GC surface was functionalized with a thiolated initiator capture probe (ICP), partially complementary to the initiator probe, an LSPR sensing chip capable of detecting miR-10b was produced. In order to confirm the conjugation efficiency, an ICP functionalized with fluorophore (cy3) at the 3-terminal (ICP-cy3) was applied. For the ICP-cy3 conjugated with the LSPR sensing chip, the fluorescence signal was inactivated owing to the quenching efficiency of the gold surface. To optimize the minimum appropriate concentration and time required for binding the ICP-cy3, different concentrations (0.5, 1, and 2 μM) and binding incubation times (30, 60, 90, and 120 min) were tested. As shown in Figure S6, the optimum ICP concentration was 1 μM, and the optimum binding time to the GC surface was 120 min.

Characterization of DNA sandwich structures

The homogeneous duplex between the ICP and initiator probe (IP) was insufficient for binding the signaling probe due to short length. Therefore, in this study, DNA sandwich structures were employed as an amplified recognition element binding the number of the LSPR signal probe. For building the DNA sandwich structure, helper probes (helper 1: H1 and helper 2: H2) composed of 18 base pairs and an additional 9 sticky end base pairs. The 9 sticky end base pairs were located at the 5' terminal of H1 (complementary to H2) and at the 3'-terminal of H2 (complementary to H1). In the presence of miR-10b, the IP was released from CP through DSN-assisted target recycling and conjugated to ICP on the GC with the partial duplex structure. Then other unconjugated region of IP was partially combined with H1 and the

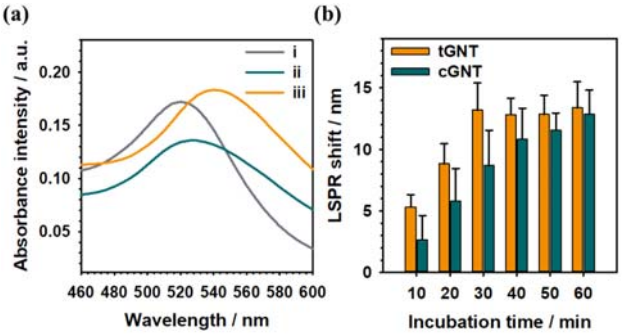

Figure 4. (a) LSPR spectra after the amplification reaction (i) without gold nanotags, (ii) ctab-capped gold nanotags(cGNTs) and (iii) tannic acid-capped gold nanotags (tGNTs). (b) The effect of the incubation time of tGNTs on the DNA sandwich structures.

newly exposed sticky end of H1 hybridized the sticky end of H2. The IP domain on the detection probe could propagate a hybridization chain reaction events between alternating H1 and H2, and finally long nicked DNA polymers could be formed. To investigate these issues, gel electrophoresis was used to characterize H1 and H2 in the presence and absence of the IP (Figure 3a-b). We used 15% polyacryl amide gel because the single strand (ICP, IP, H1 and H2) had a short length and low mass. The last part of the ladder is 50 bp, and the gel image shows that the single strand band was located 50 bp below. In the Figure 3(a), two peaks appear in lane 3, upper band was generated by the self-dimer. To demonstrate this phenomenon, we conducted the same experiment using 15% polyacrylamide gel containing urea. The role of urea is to interfere with hydrogen bonding between DNA. The last part of the ladder is 20 bp, and the gel image shows that the single strand band was located 20 bp below. It was confirmed that the self-dimer was nor formed due to the lack of hydrogen bonding, and thus one-band was formed in Figure S7. The band in lane 1 of Figure 3(b) showed that the hybridization between H1 and H2 formed a long chain. Compared to the 100 bp ladder, the H1/H2 and ICP/IP/H1/H2 bands, located in the range from 500 bp to 1500 bp, demonstrate high molecular weight and length. Moreover, when a hybridization chain reaction occurs, multiple strands and length are produced, resulting in a broad band. However, when the IP/ICP and H1/H2 were combined at a ratio of 1:1, the propagating efficiency decreased in lane 3. When the amount of H1/H2 was more than 5 times that of ICP/IP, the propagation was sufficient. Thus, the concentration at the ratio of 1:5 (ICP/IP:H1/H2) showed effective propagation by building double-stranded DNA polymers, amplifying the signal of the LSPR (lane 4).

To clarify whether the LSPR signal originated only from the adsorbed gold nanotags, we measured the absorbance of the LSPR sensing chip at various steps (Figure 3c). It can be seen that a slight red shift occurs under the condition of GC/ICP/IP/H1/H2 where DNA sandwich structures was generated. However, it was difficult to observe a significant level of LSPR red shift.

LSPR signal with the tannic acid capped gold nanotags.

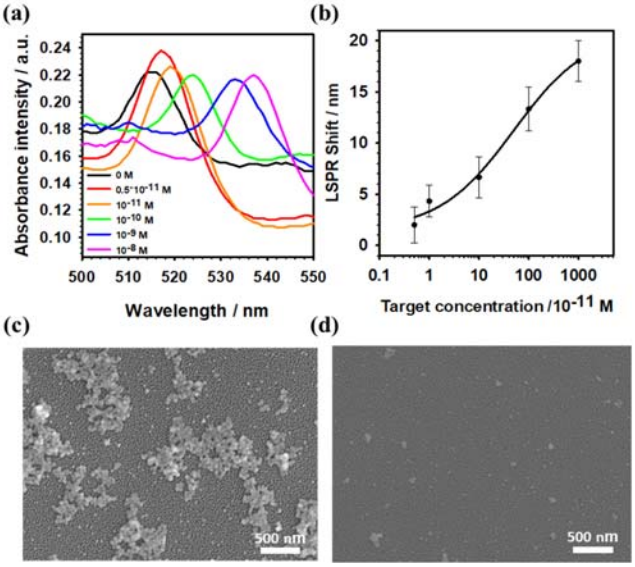

Figure 5. (a) Absorbance spectra of the HCR-tGNTs based miRNA sensors toward miR-10b and (b) Determination of limit of detection with various concentrations (5×10^{-11}, 10^{-11}, 10^{-10}, 10^{-9} and 10^{-8} M). The SEM images after incubation in the (c) presence and (d) absence of the target miR-10b.

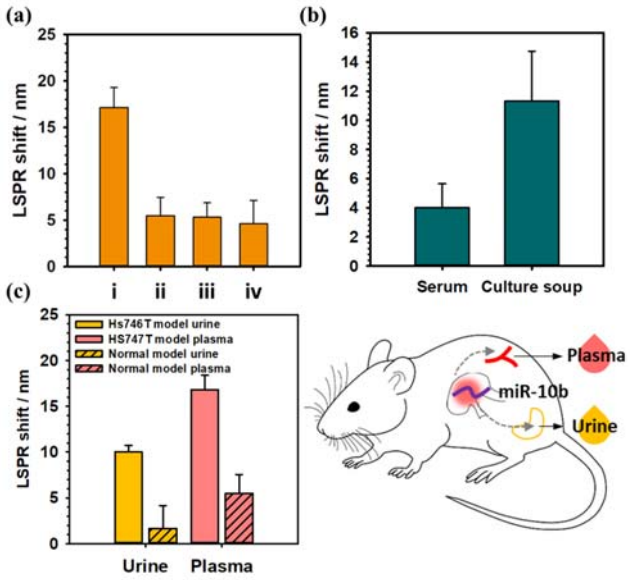

Figure 6. Detection of miRNA-10b on the localized plasmon resonance (LSPR) chip. (a) Variation of the LSPR shift in the presence of miR-10b, miR-10b with 1-base mismatches (1M-miR-10b), miR-10b with 3-base mismatches (3M-miR-10b) and miR-200b as non-complementary target. (b) LSPR shift in the serum containing 10% fatal bovine serum and culture soup of Hs746t cells. (c) LSPR shift in the mouse sample.

The assembled amount of gold nanotags on the DNA sandwich is also another important factor influencing the sensitivity of the sensors. Therefore, we developed a tannic acid capped gold nanotags to improve the performance of the sensor. The tannic acid was composed of numerous hydrophilic polyphenols that consisted of five catechols and five gallols at the termini, which could interact with the phosphate backbone of DNA via hydrogen bonding.[29-30] To verify the hypothesis, the sensor performances were compared using two types of gold nanotags: tannic acid capped gold nanotags (tGNT) and cetrimonium bromide (CTAB) positively capped gold nanotags (cGNT), which have been widely used. As shown in Figure 4a, the LSPR shift in the sensing chip using tGNT as the LSPR probe was about 2-times higher than sensing chip using cGNT at an equivalent concentration and time. This could be attributed to the hydrogen bonding interaction between the tannic acid and DNA strands.

Determination of target miRNA by LSPR

To analyze the sensitivity and detection limit of the test assay, various concentrations of serially diluted target solutions (0.5×10^{-11}, 10^{-11}, 10^{-10}, 10^{-9}, and 10^{-8} M) were used as the samples on the LSPR chip surface. The LSPR peak shift increased with an increasing concentration up to approximately the analysis capability of the target miR-10b method examined. As shown in Figure 5a, with an increase of the miR-10b concentration, the LSPR shift gradually increased. On the basis of this graph, we fitted a 4-parameter logistic model to the above data. As shown in Figure 5b, the shift value of the absorbance at 520 nm to the target miR-10b was fitted to 4-parameter logistic model to the above data. The logarithmic value was dependent on the miR-10b concentration in a range of 10^{-11} M to 10^{-8} M with a detection limit of 2.45 pM, according to the following equation: LOD = average of blank + 3(standard deviation of blank). Figure 5c-d shows a SEM image of the LSPR chip complexed with DNA sandwich structures and gGNTs. The enlargement of Figure 5c-d shows that shows that tGNT is not aggregated, however bound to DNA while retaining its original shape (Figure S8). The tGNT was bound to the DNA sandwich structures to form a cluster, which caused the LSPR signal.

To validate the selectivity of the LSPR based sensor, the system was challenged with various miRNAs as perfect matched with miR-10b, miR-10b with 1-base mismatch (1M-miR-10b), miR-10b with 3-base mismatch (3M-miR-10b) and miR-200b that was non-complementary. As shown in Figure 6a, LSPR shift in presence of 1 nM of miR-10b was observed 3.1-time, 3.2-time and 3.7-time higher than that of 10 nM of other oligomers, respectively. The LSPR shift in presence of miR-10b was observed 3.3-times, 2.7-times and 4.1-times higher than others in same concentration (10 pM), respectively (Figure S9). Therefore, this strategy was highly selective for a complementary target.

miRNA sensing in vitro mouse sample

MiRNAs regulate gene expression and are detectable in whole blood, serum, plasma, urine, and other body fluids in a highly stable form. Circulating miRNAs present a potential technological advantage because of their remarkable stability as well as their possible use in a noninvasive and rapid diagnosis. Finally, an examination was performed to determine whether the LSPR based miR-10b sensing system could be utilized to detect a target in a biological sample. First, this system was applied to cell culture soup to verify the effectiveness of the real-miRNA. An analysis of the miRNA in culture soup or exosomes can be conducted to easily determine the intracellular miRNA expression levels

in the cellular state.[31-32] To investigate the sensor performance in the biological sample, the Hs746t cell line was chosen based on their miR-10b expression level. As shown in Figure 6b, a distinguishable LSPR peak shift was observed for the miR-10b sensing system that were complementary to the miR-10b in the culture soup of the Hs746T cells. Second, the LSPR-based miR-10b sensing system was used to analyze the expression level in the miR-10b profiles of the urine and plasma samples of mice with orthotopic Hs746tT xenografts (Figure 6c). The LSPR signals measured for the urine and plasma samples of the mice with orthotopic Hs746tT xenografts were 6.0 times and 3.1 times respectively, compared with those of normal mice. Moreover, the results showed that the LSPR signal measured in the plasma sample was higher than that in the urine. These results illustrated that the LSPR based miR-10b sensing system was a promising approach for facile and sensitive detection of miRNA in body fluids.

CONCLUSION

In conclusion, we designed simple and straightforward method for sensitive detection of miRNAs in body fluid samples, which involves three steps generating a significantly enhanced LSPR signal: (i) enzyme-assisted target recycling; (ii) formation of DNA sandwich structures through sequence-specific hybridization chain reaction; (iii) gold nanotags capped with tannic acid bind to DNA sandwich structures. The detection dynamic range spans four orders of magnitude (from 5 pM to 10 nM), and the detection limit of the miR-10b was 2.45 pM. The present system showed high selectivity and can be applied to direct detection of target miR-10b in urine and plasma samples. The proposed method provides convenient alternative to standard approached for detection of circulating miRNAs in real sample and allows precision medicine and monitoring of cancer.

EXPERIMENTAL

Materials

The oligonucleotides designed in this study were purchased from Bioneer Inc. (Daejeon, Korea). Hydrogen tetrachloroaurate hydrate ($HAuCl_4 \cdot 3H_2O$), sodium citrate (SC), citric acid (CA), silver nitrate, L-ascorbic acid, tris(2-carboxyethyl)phosphine hydrochloride (TCEP), mercaptohexanol (MCH), cetyltrimethyl ammonium bromide (CTAB), sodium borohydride, and (3-aminopropyl)triethoxysilane (APTES) were obtained from Sigma-Aldrich (St. Louis, USA). Tris-HCl buffer (1 M, pH 8.8) was purchased from Biosesang, and phosphate buffered saline (PBS, 10 mM, pH 7.4) was purchased from Welgene. All other chemicals and reagents were analytical grade. The morphology of the nanoparticles was observed using high-resolution TEM (HR-TEM; JEM-2100F; JEOL, Japan) at an acceleration voltage of 200 kV and SEM (JSM-7001F, JEOL, Japan). A hybrid multimode microplate reader (Synergy 2 multimode reader; VT, USA) was used to measure the fluorescence intensity, and a UV/Vis spectrophotometer (V-650, JASCO, Japan) was used to measure the absorbance.

Synthesis of gold substrate modified with the capture probe

Before use, a gold substrate was cleaned with a piranha solution (H_2SO_4:H_2O_2 = 3:1). The capture probes were activated by a TCEP solution (0.1 M) prior to use. Then, 100 µl of 1 µM thiol-modified capture probe were applied on the cleaned gold substrate overnight in a reaction buffer (0.5 M NaCl, 10 mM Tris-HCl, 0.01 M sodium dodecyl sulfate, 0.01 M phosphate, and pH 7.4). The substrates were rinsed with 1× PBS three times to remove the unstable capture probes. The capture probe conjugation efficiency on the gold substrate was analyzed by measuring the fluorescence intensity of cy3 (excitation/emission: 540/570 nm) after the gold substrate was incubated in mercaptoethanol.

DSN-assisted target recycling

The capture probe conjugated gold substrate was prepared, and then 1× DSN buffer (50 mM Tris-HCl, pH 8.0; 5 mM $MgCl_2$, 1 mM DTT), 0.2 U DSN (dissolved in 25 mM Tris-HCl, pH 8.0; 50% glycerol), and target miRNA were incubated at 60 ℃ for 30 min. Finally, a supernatant was applied to separate the sample from the well.

Synthesis of gold nanoparticles with a 25 nm diameter

A volume of 75 mL of 2.2 mM citrate buffer (SC: CA=3:1) was heated to 100 °C with vigorous stirring. The average hydrodynamic diameters and zeta potentials of the gold nanoparticles were measured using dynamic laser scattering (ELS-Z; Otsuka Electronics, Osaka, Japan). After the solution began to boil, the solution was heated for an additional 15 min for oxidation of the citrate buffer. Then, a 0.5 mL EDTA solution (3 mM) and 0.5 mL $HAuCl_4$ solution (25 mM) were sequentially injected into the solution without a time delay. After the color of the solution changed, the solution was heated for an additional 20 min before cooling to 85 °C. At 85 °C, 0.5 mL sodium citrate (60 mM) and 0.5-mL $HAuCl_4$ (25 mM) were sequentially injected into the solution without a time delay. After 40 min, the reaction was complete.

Fabrication of the gold nanoparticles functionalized with an initiator capture probe

Cover glasses were ultrasonically cleaned in a 0.1 M KOH solution, DI water, and ethanol for 10 min, sequentially. The clean cover glasses were then immersed in 5% (v/v) APTES in ethanol for 2 h, rinsed thoroughly with ethanol, followed by DI water, and then dried with an N_2 stream. The cover glasses were then subjected to thermal annealing in an oven at 120 °C for 2 h. After thermal annealing, the cover glasses were immersed in a previously synthesized solution of gold nanoparticles with a 25 nm diameter overnight. Then, the prepared gold coated glass chips were washed with DI water and directly immersed in freshly prepared 0.5 mg/mL dopamine solution in Tris buffer (10 mM, pH 8.5) without agitation at room temperature for 30 min of polymerization. Subsequently, the LSPR chips were washed with DI water and dried with an N_2 stream. The gold coated glass chips were immersed in a 1 µM initiator capture probe (with 100 µM TCEP) dissolved in 10 mM Na_2HPO_4 citric acid and 1 M NaCl at a pH of 3.4. After 2 h of incubation at 25 ℃, the

thiolated oligonucleotides were first self-assembled on the gold coated glass chip via Au-S bonding and then immersed in 1 mM MCH solution for 2 h to remove the nonspecific adsorbed oligonucleotides and force the single strand DNA to stand up.

Polyacylamide gel electrophoresis (PAGE)
Briefly, an aliquot comprising 1μg of each oligomers (in a buffer containing 1x TBE, 10 mM Tris, 12 mM NaCl, and 1 mM $MgCl_2$) was mixed thoroughly. This solution was then heated at 95 °C for 5 min and incubated at 32 °C for 2 hours. The resulted products were examined by PAGE to confirm the presence of hybrids. The ladder information used in this experiment was as follows: 20 bp ladder; EZ Load™ 20 bp Molecular Ruler, 50 bp ladder: EBM-1004 50 bp DNA ladder marker, 100 bp: HiQ™ 100bp DNA Ladder.

Synthesis of gold the nanotags for the LSPR response
A volume of 75 mL of 0.5 mM $HAuCl_4$ solution was heated to 100 °C during vigorous stirring. After the solution began to boil, the solution was heated for an additional 15 min. Sequentially, 0.375 mL of 500 mM SC was added to the solution. The tannic acid capped gold nanotags were functionalized through a stepwise addition procedure. First, the particles were functionalized overnight with CTAB, creating CTAB capped gold nanotags. Then, the CTAB capped gold nanotags were resuspended in 10 mM tannic acid, creating tannic acid capped gold nanotags.

Hybridization chain reaction
The initiator capture probe conjugated gold nanoparticle coated glass chips were immersed in the solution and was formed after the loop amplification reaction with 5 μM H1 and H2 for 30 min at room temperature. And then, tannic acid gold nanotags were applied for 30 min at room temperature and were rinsed with PBS three times.

ASSOCIATED CONTENT

Supporting information

Sequence information of nucleic acid used in miRNA assays. X-ray photoelectron (XPS) spectra of various elemental composition in capture probe complementary with miR-10b on gold substrate. Florescence graph under various conditions to confirm enzyme activity. Transmission electron microscopy (TEM) images of gold nanoparticles. Scanning electron microscope (SEM) of gold nanoparticles conjugated on glass substrate and absorbance spectra of gold coated chip after reaction cycles. Absorbance graph of LSPR sensing chip under various polydopamine concentration. Image of gel electrophoresis to confirm single strand DNA oligomers. LSPR graph about selectivity.

Author information

Corresponding Author
*E-mail: haam@yonsei.ac.kr.
*E-mail: ymhuh@yuhs.ac.kr

Notes

The authors declare no competing financial interest.

Acknowledgment

This research was supported by BioNano Health-Guard Research Center funded by the Ministry of Science and ICT(MSIT) of Korea as Global Frontier Project (Grant number H-GUARD_2013M3A6B2078946). This research was supported by a grant of the Korea Health Technology R&D Project through the Korea Health Industry Development Institute (KHIDI), funded by the Ministry of Health & Welfare, Republic of Korea (grant number : HI18C1159).

REFERENCES

(1) Dong, H. F.; Lei, J. P.; Ding, L.; Wen, Y. Q.; Ju, H. X.; Zhang, X. J. MicroRNA: Function, Detection, and Bioanalysis. *Chem. Rev.* **2013,** *113*, 6207-6233.
(2) Bartel, D. P. MicroRNAs: Genomics, Biogenesis, Mechanism, and Function. *Cell* **2004,** *116*, 281-297.
(3) Follert, P.; Cremer, H.; Beclin, C. MicroRNAs in Brain Development and Function: A Matter of Flexibility and Stability. *Front. Mol. Neurosci.* **2014,** *7*, 5.
(4) Isaacs, S. R.; Wang, J.; Kim, K. W.; Yin, C.; Zhou, L.; Mi, Q. S.; Craig, M. E. MicroRNAs in Type 1 Diabetes: Complex Interregulation of the Immune System, beta Cell Function and Viral Infections. *Curr. Diabetes. Rep.* **2016,** *16*, 133.
(5) Freedman, J. E.; Gerstein, M.; Mick, E.; Rozowsky, J.; Levy, D.; Kitchen, R.; Das, S.; Shah, R.; Danielson, K.; Beaulieu, L.; Navarro, F. C. P.; Wang, Y. Y.; Galeev, T. R.; Holman, A.; Kwong, R. Y.; Murthy, V.; Tanriverdi, S. E.; Koupenova-Zamor, M.; Mikhalev, E.; Tanriverdi, K. Diverse Human Extracellular RNAs are Widely Detected in Human Plasma. *Nat. Commun.* **2016,** *7, 11902*.
(6) Ghai, V.; Wang, K. Recent Progress Toward The Use of Circulating MicroRNAs as Clinical Biomarkers. *Arch. Toxicol.* **2016,** *90*, 2959-2978.
(7) Kawaguchi, T.; Komatsu, S.; Ichikawa, D.; Tsujiura, M.; Takeshita, H.; Hirajima, S.; Miyamae, M.; Okajima, W.; Ohashi, T.; Imamura, T.; Kiuchi, J.; Konishi, H.; Shiozaki, A.; Okamoto, K.; Otsuji, E. Circulating MicroRNAs: A Next-Generation Clinical Biomarker for Digestive System Cancers. *Int. J. Mol. Sci.* **2016,** *17*, 1459.
(8) Rubio, M.; Bustamante, M.; Hernandez-Ferrer, C.; Fernandez-Orth, D.; Pantano, L.; Sarria, Y.; Pique-Borras, M.; Vellve, K.; Agramunt, S.; Carreras, R.; Estivill, X.; Gonzalez, J. R.; Mayor, A. Circulating MiRNAs, IsomiRs and Small RNA Clusters in Human Plasma and Breast Milk. *Plos One* **2018,** *13*, e0193527.
(9) Pantano, L.; Friedlander, M. R.; Escaramis, G.; Lizano, E.; Pallares-Albanell, J.; Ferrer, I.; Estivill, X.; Marti, E. Specific Small-RNA Signatures in The Amygdala at Premotor and Motor Stages of Parkinson's Disease Revealed by Deep Sequencing Analysis. *Bioinformatics* **2016,** *32*, 673-681.
(10) Yeri, A.; Courtright, A.; Reiman, R.; Carlson, E.; Beecroft, T.; Janss, A.; Siniard, A.; Richholt, R.; Balak, C.; Rozowsky, J.; Kitchen, R.; Hutchins, E.; Winarta, J.; Mccoy, R.; Anastasi, M.; Kim, S.; Huentelman, M.; Van Keuren-Jensen, K. Total Extracellular Small RNA Profiles from Plasma, Saliva, and Urine of Healthy Subjects. *Sci. Rep.* **2017,** *7*, 44061.
(11) Yu, X. K.; Liang, J. S.; Xu, J. R.; Li, X. S.; Xing, S.; Li, H. L.; Liu, W. L.; Liu, D. D.; Xu, J. H.; Huang, L. Z.; Du, H. L. Identification and Validation of Circulating MicroRNA Signatures for Breast Cancer Early Detection Based on Large Scale Tissue-Derived Data. *J. Breast Cancer* **2018,** *21*, 363-370.
(12) Kang, W. J.; Cho, Y. L.; Chae, J. R.; Lee, J. D.; Choi, K. J.; Kim, S. Molecular Beacon-based Bioimaging of Multiple

MicroRNAs During Myogenesis. *Biomaterials* **2011,** *32*, 1915-1922.
(13) Leone, G.; van Schijndel, H.; van Gemen, B.; Kramer, F. R.; Schoen, C. D. Molecular Beacon Probes Combined with Amplification by NASBA enable Homogeneous, Real-Time Detection of RNA. *Nucleic Acids Res.* **1998,** *26*, 2150-2155.
(14) Hutter, E.; Fendler, J. H. Exploitation of Localized Surface Plasmon Resonance. *Adv. Mater.* **2004,** *16*, 1685-1706.
(15) Willets, K. A.; Van Duyne, R. P. Localized Surface Plasmon Resonance Spectroscopy and Sensing. *Annu. Rev. Phys. Chem.* **2007,** *58*, 267-297.
(16) Joshi, G. K.; Deitz-McElyea, S.; Johnson, M.; Mali, S.; Korc, M.; Sardar, R. Highly Specific Plasmonic Biosensors for Ultrasensitive MicroRNA Detection in Plasma from Pancreatic Cancer Patients. *Nano. Lett.* **2014,** *14*, 6955-6963.
(17) Joshi, G. K.; Deitz-McElyea, S.; Liyanage, T.; Lawrence, K.; Mali, S.; Sardar, R.; Korc, M. Label-Free Nanoplasmonic-Based Short Noncoding RNA Sensing at Attomolar Concentrations Allows for Quantitative and Highly Specific Assay of MicroRNA-10b in Biological Fluids and Circulating Exosomes. *Acs Nano* **2015,** *9*, 11075-11089.
(18) Oh, S. Y.; Heo, N. S.; Shukla, S.; Cho, H. J.; Vilian, A. T. E.; Kim, J.; Lee, S. Y.; Han, Y. K.; Yoo, S. M.; Huh, Y. S. Development of Gold Nanoparticle-Aptamer-based LSPR Sensing Chips for The Rapid Detection of Salmonella Typhimurium in Pork Meat. *Sci. Rep.* **2017,** *7*, 10130.
(19) Liu, M. Y.; Yuan, M.; Lou, X. H.; Mao, H. J.; Zheng, D. M.; Zou, R. X.; Zou, N. L.; Tang, X. R.; Zhao, J. L. Label-Free Optical Detection of Single-Base Mismatches by The Combination of Nuclease and Gold Nanoparticles. *Biosens. Bioelectron.* **2011,** *26*, 4294-4300.
(20) Yin, B. C.; Liu, Y. Q.; Ye, B. C. One-Step, Multiplexed Fluorescence Detection of MicroRNAs Based on Duplex-Specific Nuclease Signal Amplification. *J. Am. Chem. Soc.* **2012,** *134*, 5064-5067.
(21) Choi, H. M. T.; Beck, V. A.; Pierce, N. A. Next-Generation in Situ Hybridization Chain Reaction: Higher Gain, Lower Cost, Greater Durability. *Acs Nano* **2014,** *8*, 4284-4294.
(22) Choi, H. M. T.; Chang, J. Y.; Trinh, L. A.; Padilla, J. E.; Fraser, S. E.; Pierce, N. A. Programmable In Situ Amplification for Multiplexed Imaging of mRNA Expression. *Nat. Biotechnol.* **2010,** *28*, 1208-1212.
(23) Sheedy, P.; Medarova, Z. The Fundamental Role of MiR-10b in Metastatic Cancer. *Am. J. Cancer Res.* **2018,** *8*, 1674-1688.
(24) Wang, Y. Y.; Ye, Z. Y.; Zhao, Z. S.; Li, L.; Wang, Y. X.; Tao, H. Q.; Wang, H. J.; He, X. J. Clinicopathologic Significance of MiR-10b Expression in Gastric Carcinoma. *Hum. Pathol.* **2013,** *44*, 1278-1285.
(25) Zhang, Y.; Liao, R. B.; Hu, L. L.; Tong, B. X.; Hao, T. F.; Wu, H. J. The MicroRNA MiR-10b as a Potentially Promising Biomarker to Predict The Prognosis of Cancer Patients: A Meta-Analysis. *Oncotarget* **2017,** *8*, 104543-104551.
(26) Bastus, N. G.; Comenge, J.; Puntes, V. Kinetically Controlled Seeded Growth Synthesis of Citrate-Stabilized Gold Nanoparticles of up to 200 nm: Size Focusing versus Ostwald Ripening. *Langmuir* **2011,** *27*, 11098-11105.
(27) Kelly, K. L.; Coronado, E.; Zhao, L. L.; Schatz, G. C. The Optical Properties of Metal Nanoparticles: The Influence of Size, Shape, and Dielectric Environment. *J. Phys. Chem. B* **2003,** *107*, 668-677.
(28) Chen, H. M.; Zhao, L.; Chen, D. Q.; Hu, W. H. Stabilization of Gold Nanoparticles on Glass Surface with Polydopamine Thin Film for Reliable LSPR Sensing. *J. Colloid Interf. Sci.* **2015,** *460*, 258-263.
(29) Labieniec, M.; Gabryelak, T. Interactions of Tannic Acid and Its Derivatives (Ellagic and Gallic acid) with Calf Thymus DNA and Bovine Serum Albumin using Spectroscopic Method. *J. Photoch. Photobio. B* **2006,** *82*, 72-78.
(30) Shin, M.; Ryu, J. H.; Park, J. P.; Kim, K.; Yang, J. W.; Lee, H. DNA/Tannic Acid Hybrid Gel Exhibiting Biodegradability, Extensibility, Tissue Adhesiveness, and Hemostatic Ability. *Adv. Funct. Mater.* **2015,** *25*, 1270-1278.
(31) Kosaka, N.; Iguchi, H.; Yoshioka, Y.; Takeshita, F.; Matsuki, Y.; Ochiya, T. Secretory Mechanisms and Intercellular Transfer of MicroRNAs in Living Cells. *J. Biol. Chem.* **2010,** *285*, 17442-17452.
(32) Han, S.; Kang, B.; Jang, E.; Ki, J.; Kim, E.; Jeong, M. Y.; Huh, Y. M.; Son, H. Y.; Haam, S. Convenient Monitoring System of Intracellular microRNA Expression during Adipogenesis via Mechanical Stimulus-Induced Exocytosis of Lipovesicular miRNA Beacon. *Adv. Healthc. Mater.* **2018,** *7*, 1701019

Table of Contents